
WEIGHT VARIANCE AMPLIFIER IMPROVES ACCURACY IN HIGH-SPARSITY ONE-SHOT PRUNING

Vincent-Daniel Yun
University of Southern California
juyoung.yun@usc.edu

Junhyuk Jo
Inha University
911whwnsgur@inha.edu

Sunwoo Lee*
Inha University
sunwool@inha.ac.kr

ABSTRACT

Deep neural networks achieve outstanding performance in visual recognition tasks, yet their large number of parameters makes them less practical for real-world applications. Recently, one-shot pruning has emerged as an effective strategy for reducing model size without additional training. However, models trained with standard objective functions often suffer a significant drop in accuracy after aggressive pruning. Some existing pruning-robust optimizers, such as SAM, and CrAM, mitigate this accuracy drop by guiding the model toward flatter regions of the parameter space, but they inevitably incur non-negligible additional computations. We propose a Variance Amplifying Regularizer (VAR) that deliberately increases the variance of model parameters during training. Our study reveals an intriguing finding that parameters with higher variance exhibit greater pruning robustness. VAR exploits this property by promoting such variance in the weight distribution, thereby mitigating the adverse effects of pruning. We further provide a theoretical analysis of its convergence behavior, supported by extensive empirical results demonstrating the superior pruning robustness of VAR.

1 Introduction

Deep neural networks have achieved remarkable success across a wide range of fields including computer vision, natural language processing, and speech recognition. It is also well known that larger models tend to have better learning capability. However, training large and deep neural networks requires enormous time and system resources, making them less practical to deploy on resource-constrained devices.

Recently, model pruning has become a popular method to reduce the model size by removing less important parameters while maintaining its accuracy Hoefler et al. [2021]. Modern deep networks have millions of parameters, and maintaining accuracy after removing weights usually requires iterative pruning with retraining Frankle and Carbin [2019]. While this approach is effective, it involves repeated optimization and heavy computation cost, making it difficult to apply in real-world applications. One-shot pruning provides a simpler and more efficient alternative Liu et al. [2019]. It removes redundant parameters in a single step after training, avoiding extra fine-tuning or multiple retraining cycles He et al. [2017]. However, models trained with standard objective functions often experience a significant drop in accuracy after one-shot pruning. Our empirical analysis suggests that this accuracy drop is closely related to the optimization process, which does not explicitly account for the distribution of model parameters. Therefore, it is imperative to develop a novel training method that encourages the model to remain robust under aggressive parameter pruning while preserving accuracy.

A desirable pruning-robust training strategy should (i) avoid costly model perturbation steps, (ii) remain compatible with standard optimizers, and (iii) promote parameter distributions that broaden during training while naturally concentrating more values near zero. In our empirical study, we find that models trained to increase parameter variance tend to exhibit greater robustness to pruning. This observation suggests that parameter variance plays a crucial role in enhancing the structural resilience of neural networks. In other words, when parameter variance is high, model accuracy can be maintained even under more aggressive parameter pruning.

*Corresponding Author. Under Review

We propose *Variance Amplifying Regularizer (VAR)*, a simple and effective neural network training strategy for one-shot pruning. VAR enlarges the variance of model parameters during training. Specifically, VAR encourages the parameters to spread more widely while increasing the number of parameters whose value is near zero. This creates a balanced parameter distribution that supports both model accuracy and pruning robustness. Unlike constraint driven optimizers, VAR works inside standard stochastic gradient descent (SGD) and does not require expensive additional computations. It can also be used together with pruning-robust optimizers such as SAM Foret et al. [2021], and CrAM Chen et al. [2023] When combined, VAR complements their loss landscape flattening effect by enhancing parameter value diversity. As a result, the model maintains accuracy even under very high pruning ratios.

Our experimental results show that when the model is trained with VAR, its accuracy is effectively preserved after one-shot pruning. We evaluate VAR across various computer vision and object segmentation benchmarks.

Our extensive empirical study shows that this increased variance improves pruning robustness. We further provide a theoretical analysis of the convergence properties of VAR for non-convex and smooth problems under mild assumptions. The analysis shows that VAR guarantees convergence while achieving the same rate as standard SGD.

Our contributions are summarized as follows.

- We introduce VAR, a simple regularization-based neural network training strategy for effective one-shot pruning.
- Our study theoretically analyzes the convergence properties of VAR under a mild assumption that the parameter variance is represented by a β_2 -smooth function.
- We also empirically demonstrate that parameter distributions can be naturally adjusted during training by penalizing the reciprocal of parameter variance, which results in a model that is more robust to pruning.

2 Related Works

Neural Network Pruning. Model pruning methods commonly drop a subset of model parameters to enable neural network training on resource-constrained systems Hoefler et al. [2021]. Early pruning approaches, such as Optimal Brain Damage LeCun et al. [1990] and Optimal Brain Surgeon Hassibi and Stork [1993] pruned parameters based on the second-order sensitivity information to minimize the increase in loss. Recently, several studies have proposed parameter magnitude-based pruning methods, typically using an L_1 -norm criterion to remove parameters with small magnitudes. Han et al. [2015] demonstrated that such unstructured, magnitude-based methods can achieve high sparsity but often require fine-tuning. In contrast, structured pruning methods remove entire channels or filters to reduce computational cost while preserving the key structural characteristics of model parameters Li et al. [2017], He et al. [2017]. More recent studies have explored dynamic and adaptive pruning approaches Gao et al. [2024], which adjust sparsity during training to balance compactness and performance.

One-Shot Pruning. One-shot pruning methods have been highlighted recently, which drop less important parameters after training at once Liu et al. [2019]. SFW Lu et al. [2022] formulates pruning as a constrained optimization problem with a K -sparse constraint. Recently, Sharpness-Aware Minimization (SAM) Foret et al. [2021] is known to not only improve generalization but also make models more robust to model pruning Na et al. [2022]. CrAM Chen et al. [2023] further enhances compression efficiency through perturbation-based optimization. However, these methods introduce additional computation or non-standard optimization steps, making them difficult to combine with other deep learning methods.

There have been several initialization-based pruning methods. SNIP Lee et al. [2019] identifies important connections by measuring each weight’s influence on the loss using a small batch of data, whereas GraSP Wang et al. [2020] preserves gradient flow to maintain signal propagation during the early training stage. SynFlow Tanaka et al. [2020] selects critical weights by maximizing synthetic information flow based on absolute weight values. Although these methods are effective for early-stage sparsification, they do not explicitly consider improving pruning robustness during training. Therefore, we exclude these initialization-based methods from our comparison.

Weight Diversity and Structural Robustness. Maintaining weight diversity which can be represented as rank has been shown to improve model stability and generalization. Soft Orthogonality (SO) Xie et al. [2017] and Double Soft Orthogonality (DSO) Bansal et al. [2018] preserve the effective rank of weights by constraining their Gram matrix toward the identity, but they rely on costly matrix-level computations that limit scalability. SRIP [Bansal et al., 2018, Candes and Tao, 2005] minimizes the spectral norm of the difference between the Gram matrix of a weight matrix and the identity matrix. These diversity-oriented regularization methods encourage models to have a higher effective rank, exploiting the maximum representational capacity. While they improve the model’s generalization, they make it difficult to distinguish important parameters from others, which in turn may harm pruning robustness. Our goal is, in

contrast, to adjust the distribution of parameter values so that a smaller subset of parameters becomes more significant than others, while maintaining the overall model accuracy.

3 Method

In this study, we introduce Variance Amplifying Regularizer (VAR) that promotes larger weight variances during training to improve model accuracies under pruning. The proposed approach adds a variance regularization term to the loss function. This encourages the weights to spread more broadly while increasing the concentration of values near zero.

Preliminaries. We denote the training dataset as $\mathcal{D} = \{(x_i, y_i)\}_{i=1}^M$, where each input $x_i \in \mathbb{R}^k$ and label y_i belongs to the label space \mathcal{Y} . A neural network is parameterized by weights $w \in \mathbb{R}^d$, and its output for input x is written as $f(x; w)$. The empirical loss is defined as $L(w) = \frac{1}{M} \sum_{i=1}^M \ell(f(x_i; w), y_i)$, where $\ell(\cdot, \cdot)$ denotes a loss function. We let $\nabla L(w)$ represent the full gradient of the loss at w , and $\nabla L_t(w)$ denote a stochastic gradient computed from a minibatch at iteration t .

Variance Amplifying Regularizer (VAR). The proposed regularizer explicitly enlarges the variance of network weights during training. Let $\mathcal{W} = \{w^{(1)}, \dots, w^{(L)}\}$ be the set of layer-wise weights. For each layer $w^{(\ell)}$, let $w^{(\ell)} = (w_1^{(\ell)}, \dots, w_{n_\ell}^{(\ell)})$ denote its individual weights. To ensure differentiability at the origin, each element is smoothly transformed as $\tilde{w}_i^{(\ell)} = \sqrt{(w_i^{(\ell)})^2 + r} \approx |w_i^{(\ell)}|$, $r = 10^{-8}$. The variance of weights for layer ℓ is computed as $\text{Var}(\tilde{w}^{(\ell)}) = \frac{1}{n_\ell} \sum_{i=1}^{n_\ell} \left(\tilde{w}_i^{(\ell)} - \frac{1}{n_\ell} \sum_{j=1}^{n_\ell} \tilde{w}_j^{(\ell)} \right)^2$. The variance amplifying penalty is then defined as

$$\psi(w) = \sum_{w^{(\ell)} \in \mathcal{W}} \frac{1}{\text{Var}(\tilde{w}^{(\ell)}) + \epsilon}, \quad (1)$$

Here, $\epsilon = 10^{-8}$ is a small constant added for numerical stability. Finally, the overall training loss is:

$$L_{total}(w) = L(w) + \lambda \psi(w). \quad (2)$$

where $\lambda > 0$ is a balancing coefficient.

The variance-regularized objective is optimized using stochastic gradient descent (SGD). At iteration t , let $\nabla L_t(w_t)$ denote the stochastic gradient of the cross-entropy loss computed on minibatch \mathcal{B}_t , and let $\nabla \psi(w_t)$ denote the gradient of the variance regularizer. The parameters are then updated using the standard SGD rule:

$$w_{t+1} = w_t - \eta(\nabla L_t(w_t) + \lambda \nabla \psi(w_t)), \quad (3)$$

where $\eta > 0$ is the learning rate.

Thus, the variance regularizer naturally integrates into the SGD framework, with its gradient contributing an additional term that pushes the weights toward configurations with larger variance. This modification preserves the standard convergence properties of SGD under β_1 -smoothness of L and the β_2 -smoothness of ψ together with standard bounded-variance conditions.

Algorithm 1 SGD with VAR pseudocode.

- 1: **Input:** λ : a balancing coefficient, T : epoch budget
 - 2: Randomly initialize w_0 .
 - 3: **for** $t \in \{1, \dots, T - 1\}$ **do**
 - 4: SGD step: $w_{t+1} = w_t - \eta(\nabla L_t(w_t) + \lambda \nabla \psi(w_t))$.
 - 5: **end for**
 - 6: **Output:** w_T
-

Algorithm. The proposed VAR regularizer can be easily integrated into the loss function of any optimizer. Algorithm 1 illustrates a standard SGD procedure that incorporates the VAR regularizer. By replacing line 4 with the parameter update rule of any other optimizer, VAR can be readily applied to the training process. This simple regularization approach is expected to serve as an appealing option for a wide range of real-world deep learning applications. In the following section, we analyze the convergence properties of Algorithm 1 under mild assumptions.

4 Theoretical Analysis

This section aims to demonstrate that the proposed weight variance amplifying regularizer (VAR) preserves the convergence property of standard stochastic gradient descent (SGD). By extending the classic SGD convergence proof Garrigos and Gower [2023], it is shown that the optimization of the total loss function $L_{\text{total}}(w) = L(w) + \lambda\psi(w)$ remains stable and convergent under the β_1 - and β_2 -smoothness assumptions and standard bounded-variance conditions. Detailed proofs are provided in the Appendix.

Assumption 1 (β_1 -smoothness). *The loss function $L : \mathbb{R}^d \rightarrow \mathbb{R}$ is β_1 -smooth, i.e., its gradient is β_1 -Lipschitz continuous $\|\nabla L(u) - \nabla L(v)\| \leq \beta_1\|u - v\|, \forall u, v \in \mathbb{R}^d$. Equivalently, for any $u, v \in \mathbb{R}^d$, the following descent lemma holds:*

$$L(u) \leq L(v) + \langle \nabla L(v), u - v \rangle + \frac{\beta_1}{2}\|u - v\|^2. \quad (4)$$

Assumption 2 (Unbiased stochastic gradient). *At each iteration t , the stochastic gradient $\nabla L_t(w_t)$ is an unbiased estimator of the true gradient:*

$$\mathbb{E}[\nabla L_t(w_t)] = \nabla L(w_t). \quad (5)$$

Assumption 3 (β_2 -smoothness of $\psi(w)$). *The regularizer $\psi : \mathbb{R}^d \rightarrow \mathbb{R}$ is assumed to be continuously differentiable. Moreover, its gradient is β_2 -Lipschitz continuous; that is, for any $w_1, w_2 \in \mathbb{R}^d$,*

$$\|\nabla\psi(w_1) - \nabla\psi(w_2)\| \leq \beta_2\|w_1 - w_2\|. \quad (6)$$

Lemma 4. *Under the β_1 -smoothness of L and the β_2 -smoothness of ψ , the combined objective $L_{\text{total}}(w) = L(w) + \lambda\psi(w)$ is β -smooth for $\beta \leq \beta_1 + \lambda\beta_2$. Together with the bounded-variance conditions $\mathbb{E}[\nabla L_t(w_t)] = \nabla L(w_t)$ and $\mathbb{E}[\|\nabla L_t(w_t) - \nabla L(w_t)\|^2] \leq \frac{\sigma^2 + \lambda^2\sigma_\psi^2}{b}$, if the step size satisfies $\eta \leq 1/\beta$, then the classic SGD update $w_{t+1} = w_t - \eta(\nabla L_t(w_t) + \lambda\nabla\psi(w_t))$ guarantees:*

$$\mathbb{E}[L(w_{t+1}) + \lambda\psi(w_{t+1})] \leq \mathbb{E}[L(w_t) + \lambda\psi(w_t)] - \frac{\eta}{2}\mathbb{E}[\|\nabla L(w_t) + \lambda\nabla\psi(w_t)\|^2] + \frac{\eta^2\beta}{2b}(\sigma^2 + \lambda^2\sigma_\psi^2). \quad (7)$$

Theorem 5. *Under the same smoothness and bounded-variance conditions stated in Lemma 4, and for a fixed step size $0 < \eta \leq 1/\beta$, the SGD update satisfies:*

$$\frac{1}{T} \sum_{t=0}^{T-1} \mathbb{E}[\|\nabla L(w_t) + \lambda\nabla\psi(w_t)\|^2] \quad (8)$$

$$\leq \frac{2}{T\eta}((L(w_0) + \lambda\psi(w_0))) - \frac{2}{T\eta}(\mathbb{E}[(L(w_T) + \lambda\psi(w_T))]) + \frac{\eta\beta\sigma^2}{2b} + \frac{\lambda^2\eta\beta\sigma_\psi^2}{2b} \quad (9)$$

Corollary 6. *Under the same smoothness and bounded-variance assumptions stated in Lemma 4, and assuming further that L_{total} is bounded below by $L_{\text{total}}^{\text{inf}} > -\infty$, let the step size be constant $\eta = \frac{c}{\sqrt{T}}$ with $0 < c \leq \frac{1}{\beta}$. Then the SGD iterates satisfy:*

$$\frac{1}{T} \sum_{t=0}^{T-1} \mathbb{E}[\|\nabla L(w_t) + \lambda\nabla\psi(w_t)\|^2] \leq \frac{2((L(w_0) + \lambda\psi(w_0)) - L_{\text{total}}^{\text{inf}})}{c} T^{-1/2} + \frac{\beta c}{2b}(\sigma^2 + \lambda^2\sigma_\psi^2) T^{-1/2}.$$

Remark 1. Under Assumption 3 on the differentiable variance regularizer, the proposed objective function in (2) preserves the convergence guarantee of standard SGD. Although the variance term increases due to the additional σ_ψ^2 term, the overall convergence rate remains $\mathcal{O}(1/\sqrt{T})$, matching the rate reported in previous works Ghadimi and Lan [2013], Yu et al. [2019]. In other words, when T is sufficiently large, the impact of VAR on the convergence speed becomes negligible.

Remark 2. The smoothed transformation of the absolute value $\tilde{w}_i = \sqrt{w_i^2 + r}$ with $r > 0$ is differentiable for all weight values. Since the layer-wise variance $\text{Var}(\tilde{w}^{(\ell)})$ is a differentiable function of the corresponding layer parameters $w^{(\ell)}$, each reciprocal term $1/(\text{Var}(\tilde{w}^{(\ell)}) + \epsilon)$ is also differentiable. Because the regularizer $\psi(w)$ is defined as the sum of these layer-wise terms, it is differentiable with respect to the full parameter vector w . In our analysis, we further assume that ψ satisfies the β_2 -smoothness condition stated in Assumption 3.

Remark 3. Since λ is set to a small value (e.g., 10^{-5}), the additional term on the right-hand side becomes small, and its effect on the overall bound is practically negligible.

Corollary 7 (Diminishing step size). *Under the same smoothness and bounded-variance assumptions stated in Lemma 4, and assuming further that the total objective $L(w) + \lambda\psi(w)$ is bounded below by $L_{\text{total}}^{\text{inf}} > -\infty$, consider SGD with a diminishing step-size sequence $(\eta_t)_{t \geq 0}$ satisfying:*

$$0 < \eta_t \leq \frac{1}{\beta}, \quad \sum_{t=0}^{\infty} \eta_t = \infty, \quad \sum_{t=0}^{\infty} \eta_t^2 < \infty. \quad (10)$$

Then the (step-size)–weighted average of squared gradients vanishes when $\nabla L_{\text{total}}(w_t) = \nabla L(w_t) + \lambda \nabla \psi(w_t)$:

$$\lim_{T \rightarrow \infty} \frac{1}{\sum_{t=0}^{T-1} \eta_t} \sum_{t=0}^{T-1} \eta_t \mathbb{E} [\|\nabla L_{\text{total}}(w_t)\|^2] = 0. \quad (11)$$

In particular,

$$\liminf_{T \rightarrow \infty} \min_{0 \leq t \leq T-1} \mathbb{E} [\|\nabla L_{\text{total}}(w_t)\|^2] = 0 \quad (12)$$

Therefore, there exists a subsequence along which the expected squared gradient converges to 0.

Remark 4. Corollary 7 indicates that, as the learning rate approaches zero, SGD drives the model parameters toward a stationary point of the objective. This behavior is consistent with that of standard SGD, confirming that the proposed regularizer does not alter the asymptotic convergence property.

The above analysis establishes that the proposed variance amplifying regularizer does not affect the stability or convergence behavior of standard stochastic gradient descent. Under common smoothness and bounded-variance assumptions, the total objective $L_{\text{total}}(w) = L(w) + \lambda\psi(w)$ converges to a stationary point with the same $\mathcal{O}(1/\sqrt{T})$ rate as standard SGD. The regularizer introduces only a small additional variance term proportional to λ^2 , which is negligible in practice. Therefore, incorporating VAR maintains the theoretical guarantees of SGD.

5 Experimental Results

5.1 Experimental Settings

We evaluate VAR on multiple benchmark datasets for both image classification and segmentation using diverse neural networks. For image classification, we use CIFAR-10 Krizhevsky [2009], CIFAR-100 Krizhevsky [2009], SVHN Netzer et al. [2011], and Tiny-ImageNet CS231N [2015] with ResNet-18 He et al. [2016], ResNet-50 He et al. [2016], WideResNet-28-10 Zagoruyko and Komodakis [2016], and ViT-B/32 Dosovitskiy et al. [2021], respectively. Only ViT-B/32 models are initialized from ImageNet pretrained weights. For image segmentation, we train a ResNet-50–UNet Ronneberger et al. [2015] model on the LGG Brain MRI dataset Buda et al. [2019] using only tumor positive samples and their corresponding ground truth masks.

Table 1: Summary of datasets, network architectures, and training settings used in the experiments.

Task	Model	Dataset	# Epochs	Batch Size	λ
Classification	ResNet-18 He et al. [2016]	CIFAR-10 Krizhevsky [2009]	200	128	1e-5
	ResNet-50 He et al. [2016]	SVHN Netzer et al. [2011]	200	128	1e-5
	WideRes28-10 Zagoruyko and Komodakis [2016]	CIFAR-100 Krizhevsky [2009]	200	128	1e-5
	ViT-B/32 Dosovitskiy et al. [2021]	CIFAR-100 Krizhevsky [2009]	200	128	1e-2
	ViT-B/32 Dosovitskiy et al. [2021]	Tiny-ImageNet CS231N [2015]	200	128	1e-2
Segmentation	Res50-Unet Ronneberger et al. [2015]	LGG MRI Buda et al. [2019]	200	64	1e-5

Table 1 summarizes the datasets, architectures, and training configurations. The batch size is set to 128 for classification and 64 for segmentation. For classification tasks, we follow the original configurations of SFW Lu et al. [2022], CrAM Chen et al. [2023], and SAM Foret et al. [2021]. The SAM and SGD experiments use the same training setup as SAM Foret et al. [2021] for fair comparison. For ViT-B/32 models, the initial learning rate is set to 0.001 with a step decay factor of 0.5 every 50 epochs. In segmentation, the initial learning rate is set to 0.001 with a step decay factor of 0.5 every 50 epochs and early stopping is applied. Please find more detailed hyper-parameter settings in the Appendix.

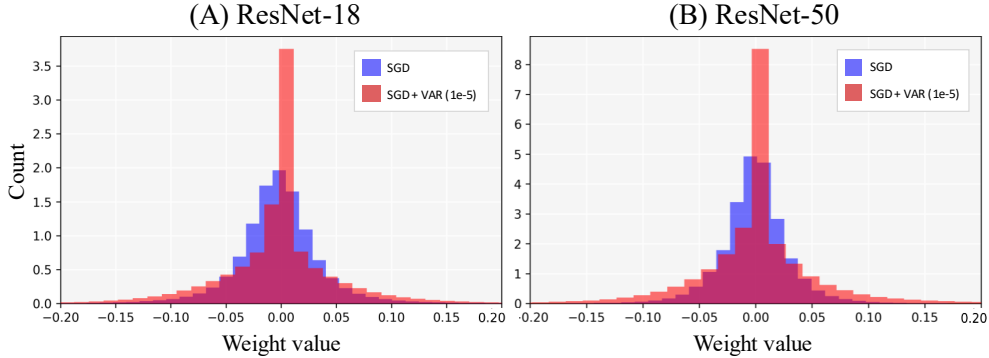


Figure 1: Weight parameters’ distribution comparison of models trained with standard SGD (blue) and SGD with the proposed Variance Amplifying Regularizer (red, $\lambda = 1e-5$). (A) ResNet-18 on CIFAR-10, (B) ResNet-50 on SVHN, and (C) WideResNet-28-10 on CIFAR-100. Across all architectures, applying Variance Amplifying Regularizer (VAR) under the same SGD training setting broadens the weight distribution.

Evaluation Metrics. For classification tasks, we report test accuracy as the primary performance measure. For segmentation tasks, we report the F1 score, Tversky index, and Hausdorff distance. The Tversky index asymmetrically penalizes false positives and false negatives, and higher values indicate better segmentation quality. The Hausdorff distance measures the maximum boundary deviation between the prediction and the ground truth, and lower values indicate more precise boundary alignment.

One-shot Pruning Method. All pruning is performed in a *one-shot* method, applied once after full training without retraining or fine-tuning. In convolutional networks, convolutional weights are globally pruned using an L_1 magnitude threshold. For vision transformers, pruning is applied to the self-attention and feed-forward modules using two configurations: (P1) equal pruning across Query, Key, Value, Projection, and FFN layers, and (P2) slightly adjusts the ratio by pruning FFN layers 3% more while pruning the remaining (QKV and Projection) layers proportionally less, maintaining the same overall pruning rate.

Weight Variance Analysis. To investigate the effect of the proposed Variance Amplifying Regularizer (VAR), the weight distributions of models trained with and without VAR were analyzed. As shown in Figure 1, applying VAR ($\lambda = 1 \times 10^{-5}$) under the same SGD training setting leads to a broader weight distribution and increases the proportion of weights near zero across all architectures. This indicates that the regularizer effectively expands the overall variance of model parameters while increasing the density of values near zero, leading to a distribution that is broader and more structured. As shown later in Section 5.5, a larger λ further increases parameter variance and directly controls how widely the model spreads its weights.

5.2 Classification Results

Each baseline is evaluated with and without the proposed Variance Amplifying Regularizer (VAR), denoted as “w/o” and “w,” respectively. Results are reported across different architectures and pruning ratios.

CNN Training. Table 2 summarizes the classification performance on CIFAR-10/100 and SVHN using multiple CNN architectures. Across all pruning levels, models trained with VAR achieve higher accuracy and exhibit improved stability after one-shot pruning. Overall, VAR allows CNNs to maintain discriminative capability even under high sparsity pruning conditions.

ViT Fine-Tuning. Table 3 presents the results on ViT-B/32 for CIFAR-100 and Tiny-ImageNet under different pruning ratios. Here, P1 denotes uniform pruning across all Query, Key, Value, Projection, and FFN layers, while P2 applies 3% higher pruning to FFN layers and proportionally less to the others, maintaining the same overall sparsity. As the pruning ratio increases to 80%, the accuracy gap between baseline and VAR-trained models becomes more evident. While baseline models show a notable drop in accuracy at higher sparsity, models trained with VAR maintain relatively stable performance across datasets.

Pruning Rate	Method VAR (Ours)	CIFAR-10		SVHN		CIFAR-100	
		ResNet-18		ResNet-50		WideRes-28-10	
		w/o	w	w/o	w	w/o	w
Dense	SGD	92.75	92.76	94.44	94.56	75.93	75.82
	SFW	92.54	92.34	95.79	95.80	63.01	64.91
	CrAM	94.19	93.86	95.97	95.79	76.29	75.86
	SAM	95.19	94.01	96.96	95.98	78.43	79.51
92%	SGD	31.60	70.18	9.16	7.77	2.86	10.88
	SFW	92.54	92.32	95.82	95.79	63.0	64.90
	CrAM	86.54	92.14	78.51	90.51	25.87	55.47
	SAM	87.20	93.91	73.37	95.98	4.26	77.95
94%	SGD	26.10	50.25	9.15	6.37	1.00	4.00
	SFW	92.22	92.29	95.73	95.77	59.59	62.18
	CrAM	80.40	89.47	53.30	82.65	7.43	31.56
	SAM	76.29	93.77	24.98	95.98	1.94	73.97
96%	SGD	19.69	21.53	9.15	6.37	1.00	1.00
	SFW	84.15	89.93	18.20	95.49	1.00	18.77
	CrAM	66.66	81.72	27.78	31.26	3.06	7.73
	SAM	48.36	92.08	9.74	95.99	1.00	56.56

Table 2: Accuracy comparison (%) across different pruning rates and datasets (CIFAR-10/100, SVHN) using various CNN architectures, with and without VAR, denoted as “w/o” and “w.”

Pruning Rate	Method VAR (Ours)	CIFAR-100				Tiny-ImageNet			
		ViT-B/32 (P1)		ViT-B/32 (P2)		ViT-B/32 (P1)		ViT-B/32 (P2)	
		w/o	w	w/o	w	w/o	w	w/o	w
Dense	SGD	89.84	89.75	89.84	88.75	86.89	86.72	86.89	86.72
	SFW	N/A	N/A	N/A	N/A	N/A	N/A	N/A	N/A
	CrAM	88.71	87.82	88.71	87.82	87.08	87.12	87.08	87.12
	SAM	87.36	87.82	87.36	87.82	87.29	87.11	87.29	87.11
60%	SGD	86.30	88.58	85.36	88.19	82.90	85.43	81.77	82.86
	SFW	N/A	N/A	N/A	N/A	N/A	N/A	N/A	N/A
	CrAM	86.33	87.08	85.73	86.81	83.29	84.46	82.23	83.67
	SAM	84.83	87.82	84.40	87.83	82.79	85.77	81.50	83.98
70%	SGD	78.33	85.66	75.27	84.37	73.79	79.23	69.55	76.86
	SFW	N/A	N/A	N/A	N/A	N/A	N/A	N/A	N/A
	CrAM	82.80	85.47	81.94	84.26	75.36	77.14	73.29	75.18
	SAM	80.29	87.97	78.30	87.50	73.22	79.82	69.15	77.47
80%	SGD	51.13	73.69	41.68	64.33	39.59	60.15	29.94	49.94
	SFW	N/A	N/A	N/A	N/A	N/A	N/A	N/A	N/A
	CrAM	70.31	79.29	64.27	76.73	47.25	57.12	37.34	43.14
	SAM	64.11	84.95	55.63	83.69	41.57	59.40	31.96	49.71

Table 3: Accuracy comparison (%) across different pruning rates and datasets (CIFAR-100, Tiny-ImageNet on ViT-B/32, with and without the proposed Variance Amplifying Regularizer (VAR), denoted as “w/o” and “w.” SFW results are marked as “N/A” since SFW is not applicable to ViT architectures.

Model	Pruning Ratio Method	Dense			85%			88%		
		Test F1	Test Tversky	H-Dist.	Test F1	Test Tversky	H-Dist.	Test F1	Test Tversky	H-Dist.
ResNet-50-Unet	SGD	0.9284	0.9439	12.55	0.3083	0.3848	108.78	-	-	-
	SGD + VAR	0.9258	0.9377	13.14	0.5136	0.5294	97.41	0.5280	0.5253	87.55
	SFW	0.9295	0.9452	9.18	0.5017	0.4480	89.97	0.1435	0.1100	84.42
	SFW + VAR	0.9191	0.9346	13.84	0.7938	0.7928	32.61	0.7210	0.6909	31.78
	CrAM	0.9163	0.9366	19.11	0.1877	0.2758	110.31	0.2811	0.2888	105.89
	CrAM + VAR	0.8994	0.9245	21.12	0.4066	0.5005	106.17	0.3264	0.3345	103.99
	SAM	0.9264	0.9378	9.26	0.3903	0.4399	107.11	0.2786	0.2587	100.13
	SAM + VAR	0.9267	0.9442	9.02	0.7244	0.8024	54.07	0.7018	0.7791	58.12

Table 4: Quantitative comparison of segmentation performance on the LGG MRI dataset using the ResNet-50-UNet architecture under different pruning ratios (Dense, 85%, and 88%). The results report Test F1, Tversky Index, and Hausdorff Distance (H-Dist.) for each method, with and without the proposed Variance Amplifying Regularizer (VAR). “-” indicates that SGD failed to produce segmentation results after pruning.

Under the same training conditions, VAR combined with SGD achieves higher pruning robustness than methods such as SAM, and CrAM without VAR. Unlike these approaches, VAR does not require additional gradient perturbation or curvature estimation, resulting in lower computational overhead. This suggests that promoting weight variance during training contributes to maintaining model accuracy under high sparsity in transformer architectures while offering a more computationally efficient alternative.

5.3 Segmentation Results

The proposed Variance Amplifying Regularizer (VAR) was further evaluated on the LGG Brain MRI dataset using the ResNet-50-UNet architecture. As shown in Table 4, applying VAR results in more stable segmentation performance under one-shot pruning. Across all methods, models trained with VAR achieve higher F1 and Tversky scores and lower Hausdorff distances, indicating improved robustness to pruning. Even at high pruning ratios of 85% and 88%, VAR-regularized models retain meaningful segmentation accuracy, while baseline models show a clear decline. Figure 2 further illustrates that VAR preserves clearer and more complete lesion boundaries after pruning. Overall, integrating VAR during training enhances the stability of segmentation models under high pruning rate without additional fine-tuning.

5.4 Generalization Effects

We analyze how VAR affects generalization on CIFAR-10 using ResNet-18. The training runs for 300 epochs with a batch size of 1,024. Figure 3 shows that both SGD and SAM perform better when VAR is applied. The largest Hessian eigenvalue represents the maximum curvature of the loss surface. It measures how sharply the loss changes along the steepest direction in the parameter space. A smaller Hessian eigenvalue indicates that the local curvature is lower,

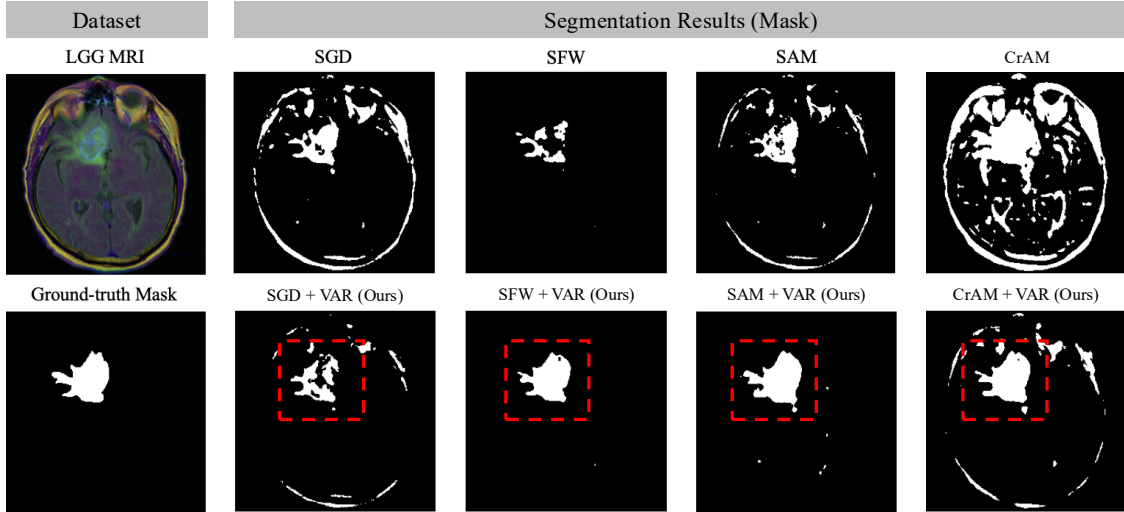


Figure 2: Qualitative segmentation results on the LGG MRI dataset using the ResNet-50-UNet architecture under 85% pruning. Each column corresponds to a different methods, with and without our proposed Variance Amplifying Regularizer (VAR).

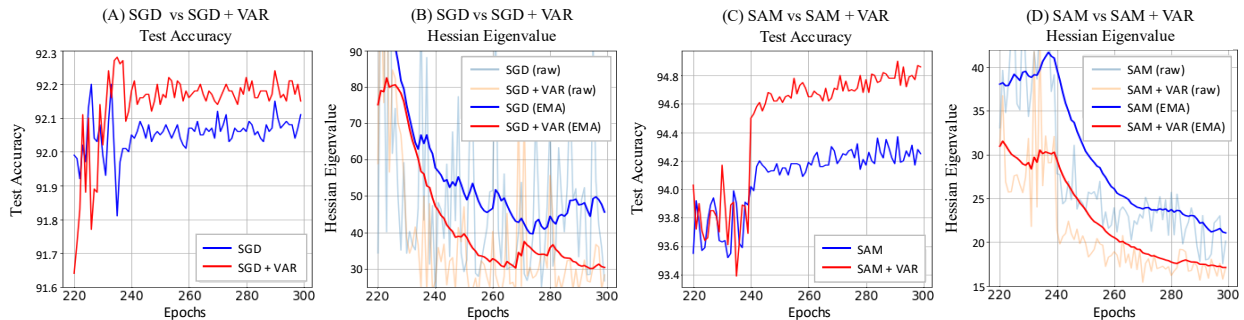


Figure 3: Comparison of SGD and SAM with and without the proposed Variance Amplifying Regularizer (VAR) on CIFAR-10 using ResNet-18 (training batch size 1024, trained for 300 epochs). (A,C) show test accuracy over training epochs; (B,D) show Hessian eigenvalue, which represents the maximum curvature of the loss surface. For (B,D), both raw traces (faint) and EMA-smoothed curves (bold) are presented, where the EMA is an exponential moving average applied across epochs to reduce stochastic noise.

meaning the loss landscape is flatter and the model is less sensitive to small weight perturbations. This property is closely related to better generalization, as flatter minima are known to yield more stable solutions that perform well on unseen data Keskar et al. [2016].

In our experiments, both SGD+VAR and SAM+VAR consistently show lower eigenvalue values than their baselines. The decrease in curvature aligns with higher and more stable test accuracy across 300 epochs. This suggests that VAR encourages the model to converge toward flatter and more generalizable regions of the loss surface, improving both robustness and performance.

5.5 Ablation Study

Tables 5 and 6 present ablation studies on the effect of the regularization coefficient λ on model performance and parameter variance. As λ increases, the variance $Var(w)$ of entire model parameters also increases, confirming that the proposed regularizer explicitly controls the spread of the weights during training.

For CNNs (ResNet-18 on CIFAR-10), Table 6 shows that $\lambda = 1 \times 10^{-5}$ provides stable performance across most pruning ratios without destabilizing optimization. For Vision Transformers (ViT-B/32 on CIFAR-100), Table 5 shows

that a relatively larger coefficient $\lambda = 1 \times 10^{-2}$ provides good pruning resilience under both P1- and P2-pruning settings. This indicates that transformer-based architectures benefit from stronger regularization due to their large model sizes.

Pruning Rate	λ $Var(w)$	P1-Pruning						P2-Pruning					
		N/A	1e-5	1e-4	1e-3	1e-2	1e-1	N/A	1e-5	1e-4	1e-3	1e-2	1e-1
Dense		89.84	90.00	90.15	89.62	88.75	85.23	89.84	90.00	90.15	89.62	88.75	85.23
60%		86.30	86.68	87.29	88.23	88.58	85.23	85.36	85.79	86.58	87.82	88.19	85.27
70%		78.33	78.76	80.45	84.83	85.66	83.81	75.27	75.58	77.83	83.36	84.37	82.08
80%		51.13	52.93	55.48	69.63	73.69	68.11	41.68	43.47	44.16	61.43	64.33	52.75

Table 5: Performance comparison of ImageNet-pretrained Vision Transformer (ViT-B/32) models on CIFAR-100 under different pruning and regularization settings (λ). P1-Pruning applies an equal pruning ratio across all Query, Key, Value, Projection, and FFN layers, while P2-Pruning prunes FFN layers 3% more and the remaining layers proportionally less, having the same overall pruning rate.

Pruning Rate	λ $Var(w)$	NA	1e-6	5e-6	1e-5	5e-5	1e-4	5e-4	1e-3
Dense		92.75	93.14	91.87	92.76	92.79	91.62	90.54	90.66
60%		91.66	92.93	91.61	92.0	92.61	91.59	90.44	90.54
70%		91.66	92.40	91.39	91.82	92.05	90.72	89.79	90.08
80%		85.93	90.36	89.77	91.14	90.29	85.86	84.75	82.16
90%		43.57	68.55	77.00	80.51	76.73	64.87	66.22	58.22
92%		31.60	57.53	65.47	70.18	68.05	53.47	52.11	47.39
94%		26.10	41.02	51.0	50.25	49.56	41.62	31.5	35.25
96%		19.69	24.53	36.79	21.53	20.60	21.72	12.75	20.18

Table 6: Performance comparison across different regularization coefficient (λ) values on CIFAR-10 with ResNet-18. The column labeled *NA* denotes the baseline without the variance regularizer.

Overall, these results demonstrate that λ effectively serves as a controllable factor determining the strength of variance regularization. As λ increases, the regularization effect becomes stronger, enhancing variance amplification but potentially introducing a trade-off between improved pruning robustness and training stability. In our experiments, we set $\lambda = 1 \times 10^{-5}$ for CNNs and $\lambda = 1 \times 10^{-2}$ for ViTs to achieve consistent and balanced regularization strength.

6 Discussion

Our study finds that the increase in parameter variance helps preserve the model’s inherent knowledge and maintain its accuracy after model pruning. Specifically, training with the variance regularizer changes how parameter magnitudes are distributed across the network. The parameter values spread over a wider numerical range and more parameters move toward zero. This redistribution forms a clearer separation between small and large weights allowing pruning to focus more precisely on less informative parameters. When parameters with small magnitudes are removed, the functional change in the network becomes smaller and the model maintains higher accuracy after pruning.

7 Conclusion

This work introduces a parameter variance amplifying regularizer (VAR) that enhances pruning robustness without modifying standard optimization pipelines. The proposed regularizer increases the variance of model parameters during training, leading to broader parameter distributions that better tolerate pruning-induced perturbations. Our theoretical analysis confirms that incorporating VAR preserves the convergence guarantees of SGD under standard smoothness assumptions. Extensive experiments across classification and segmentation tasks also demonstrate that VAR consistently improves pruning resilience for both convolutional and transformer architectures, maintaining accuracy even at high sparsity levels. These results suggest that controlling weight variance is an effective and computationally efficient approach for improving structural robustness.

Limitations and Future Work. In this work, we empirically validated the improved generalization performance by analyzing the principal Hessian eigenvalues. Therefore, understanding the impact of VAR on the generalization bound is crucial for providing a theoretical performance guarantee. We leave the analysis of its generalization bound as an important direction for future work.

References

- Torsten Hoefler, Dan Alistarh, Tal Ben-Nun, Nikoli Dryden, and Alexandra Peste. Sparsity in deep learning: pruning and growth for efficient inference and training in neural networks. In *The Journal of Machine Learning Research*, 2021.
- Jonathan Frankle and Michael Carbin. The lottery ticket hypothesis: Finding sparse, trainable neural networks. In *International Conference on Learning Representations*, 2019.
- Zhuang Liu, Mingjie Sun, Tinghui Zhou, Gao Huang, and Trevor Darrell. Rethinking the value of network pruning. In *International Conference on Learning Representations*, 2019.
- Yihui He, Xiangyu Zhang, and Jian Sun. Channel pruning for accelerating very deep neural networks. In *International Conference on Computer Vision*, 2017.
- Pierre Foret, Ariel Kleiner, Hossein Mobahi, and Behnam Neyshabur. Sharpness-aware minimization for efficiently improving generalization. In *International Conference on Learning Representations*, 2021.
- Liang Chen, Xiaoling Li, and Xiaolong Hu. Cram: Sharpness-aware minimization for efficient model compression. In *International Conference on Learning Representations*, 2023.
- Yann LeCun, John S. Denker, and Sara A. Solla. Optimal brain damage. In *Advances in Neural Information Processing Systems (NeurIPS)*, volume 2, pages 598–605. Morgan Kaufmann, 1990.
- Babak Hassibi and David G. Stork. Second order derivatives for network pruning: Optimal brain surgeon. *Advances in Neural Information Processing Systems (NeurIPS)*, 5:164–171, 1993.
- Song Han, Jeff Pool, John Tran, and William Dally. Learning both weights and connections for efficient neural network. In *Advances in Neural Information Processing Systems*, 2015.
- Hao Li, Asim Kadav, Igor Durdanovic, Hanan Samet, and Hans Peter Graf. Pruning filters for efficient convnets. In *International Conference on Learning Representations*, 2017.
- Zheyuan Gao, Yan Zhang, Wei Lu, Mingming Ma, Xiaolin Hu, and Ming-Ming Cheng. Bilevelpruning: Unified dynamic and static channel pruning for convolutional neural networks. In *Proceedings of the IEEE/CVF Conference on Computer Vision and Pattern Recognition (CVPR)*, pages 18873–18883, 2024.
- Miao Lu, Xiaolong Luo, Tianlong Chen, Wuyang Chen, Dong Liu, and Zhangyang Wang. Learning pruning-friendly networks via frank-wolfe: One-shot, any-sparsity, and no retraining. In *International Conference on Learning Representations*, 2022.
- Clara Na, Sanket Vaibhav Mehta, and Emma Strubell. Train flat, then compress: Sharpness-aware minimization learns more compressible models. In *Findings of the Association for Computational Linguistics: EMNLP 2022*, pages 4909–4936, December 2022.
- Namhoon Lee, Thalaisyasingam Ajanthan, and Philip HS Torr. Snip: Single-shot network pruning based on connection sensitivity. In *International Conference on Learning Representations*, 2019.
- Chaoqi Wang, Guodong Zhang, and Roger Grosse. Picking winning tickets before training by preserving gradient flow. In *International Conference on Learning Representations*, 2020.
- Hidenori Tanaka, Daniel Kunin, Daniel L. K. Yamins, and Surya Ganguli. Pruning neural networks without any data by iteratively conserving synaptic flow. In *Advances in Neural Information Processing Systems*, 2020.
- Di Xie, Jiang Xiong, and Shiliang Pu. All you need is beyond a good init: Exploring better solution for training extremely deep convolutional neural networks with orthonormality and modulation. In *2017 IEEE Conference on Computer Vision and Pattern Recognition (CVPR)*, 2017.
- Nitin Bansal, Xiaohan Chen, and Zhangyang Wang. Can we gain more from orthogonality regularizations in training deep cnns? In *Proceedings of the 32nd International Conference on Neural Information Processing Systems*, 2018.
- Emmanuel J Candes and Terence Tao. Decoding by linear programming. *IEEE transactions on information theory*, 51(12):4203–4215, 2005.
- Guillaume Garrigos and Robert M. Gower. Handbook of convergence theorems for (stochastic) gradient methods. In *Arxiv Preprint*, 2023.

-
- Saeed Ghadimi and Guanghui Lan. Stochastic first-and zeroth-order methods for nonconvex stochastic programming. *SIAM journal on optimization*, 23(4):2341–2368, 2013.
- Hao Yu, Rong Jin, and Sen Yang. On the linear speedup analysis of communication efficient momentum sgd for distributed non-convex optimization. In *International Conference on Machine Learning*, pages 7184–7193. PMLR, 2019.
- Alex Krizhevsky. Learning multiple layers of features from tiny images. Technical report, University of Toronto, 2009.
- Yuval Netzer, Tao Wang, Adam Coates, Alessandro Bissacco, Bo Wu, and Andrew Y. Ng. Reading digits in natural images with unsupervised feature learning. In *NIPS Workshop on Deep Learning and Unsupervised Feature Learning*, 2011.
- Stanford CS231N. Tiny imagenet visual recognition challenge, 2015.
- Kaiming He, Xiangyu Zhang, Shaoqing Ren, and Jian Sun. Deep residual learning for image recognition. In *IEEE Conference on Computer Vision and Pattern Recognition (CVPR)*, 2016.
- Sergey Zagoruyko and Nikos Komodakis. Wide residual networks. In *British Machine Vision Conference (BMVC)*, 2016.
- Alexey Dosovitskiy, Lucas Beyer, Alexander Kolesnikov, Dirk Weissenborn, Xiaohua Zhai, Thomas Unterthiner, Mostafa Dehghani, Matthias Minderer, Georg Heigold, Sylvain Gelly, Jakob Uszkoreit, and Neil Houlsby. An image is worth 16x16 words: Transformers for image recognition at scale. In *International Conference on Learning Representations*, 2021.
- Olaf Ronneberger, Philipp Fischer, and Thomas Brox. U-net: Convolutional networks for biomedical image segmentation. In *International Conference on Medical Image Computing and Computer-Assisted Intervention (MICCAI)*, 2015.
- Mateusz Buda, Ashirbani Saha, and Maciej A. Mazurowski. Association of genomic subtypes of lower-grade gliomas with shape features automatically extracted by a deep learning algorithm. *Computers in Biology and Medicine*, 2019.
- Nitish Shirish Keskar, Dheevatsa Mudigere, Jorge Nocedal, Mikhail Smelyanskiy, and Ping Tak Peter Tang. On large-batch training for deep learning: Generalization gap and sharp minima. *arXiv preprint arXiv:1609.04836*, 2016.

Appendix

This appendix provides additional materials that complement the main paper. It includes the full theoretical analysis supporting the convergence behavior of our Variance Amplifying Regularizer (VAR), extended implementation details for all experiments, and additional qualitative and quantitative results that further illustrate the effect of VAR. The appendix is organized as follows:

- **Appendix A:** Theoretical analysis and proofs for the proposed VAR.
- **Appendix B:** Experimental setup, implementation details, and evaluation metrics.
- **Appendix C:** Extended experimental results.
- **Appendix D:** PyTorch implementation of the Variance Amplifying Regularizer.

A Theoretical Analysis

In this section, we provide the detailed proofs of the lemmas and corollaries presented in the main paper. Specifically, we establish that adding the Variance Amplifying Regularizer (VAR) preserves the convergence properties of stochastic gradient descent under standard smoothness and bounded-variance assumptions.

Assumption 1 (β_1 -smoothness). *The loss function $L : \mathbb{R}^d \rightarrow \mathbb{R}$ is β_1 -smooth, i.e., its gradient is β_1 -Lipschitz continuous $\|\nabla L(u) - \nabla L(v)\| \leq \beta_1 \|u - v\|, \forall u, v \in \mathbb{R}^d$. Equivalently, for any $u, v \in \mathbb{R}^d$, the following descent lemma holds:*

$$L(u) \leq L(v) + \langle \nabla L(v), u - v \rangle + \frac{\beta_1}{2} \|u - v\|^2. \quad (13)$$

Assumption 2 (Unbiased stochastic gradient). *At each iteration t , the stochastic gradient $\nabla L_t(w_t)$ is an unbiased estimator of the true gradient:*

$$\mathbb{E}[\nabla L_t(w_t)] = \nabla L(w_t). \quad (14)$$

Assumption 3 (β_2 -smoothness of $\psi(w)$). *The regularizer $\psi : \mathbb{R}^d \rightarrow \mathbb{R}$ is assumed to be continuously differentiable. Moreover, its gradient is β_2 -Lipschitz continuous; that is, for any $w_1, w_2 \in \mathbb{R}^d$,*

$$\|\nabla \psi(w_1) - \nabla \psi(w_2)\| \leq \beta_2 \|w_1 - w_2\|. \quad (15)$$

We now provide the proofs for all the proposed lemmas and the theorem as follows.

Lemma 4. *Under the β_1 -smoothness of L and the β_2 -smoothness of ψ , the combined objective $L_{\text{total}}(w) = L(w) + \lambda\psi(w)$ is β -smooth for $\beta \leq \beta_1 + \lambda\beta_2$. Together with the bounded-variance conditions $\mathbb{E}[\nabla L_t(w_t)] = \nabla L(w_t)$ and $\mathbb{E}[\|\nabla L_t(w_t) - \nabla L(w_t)\|^2] \leq \frac{\sigma^2 + \lambda^2 \sigma_\psi^2}{b}$, if the step size satisfies $\eta \leq 1/\beta$, then the classic SGD update $w_{t+1} = w_t - \eta(\nabla L_t(w_t) + \lambda \nabla \psi(w_t))$ guarantees:*

$$\mathbb{E}[L(w_{t+1}) + \lambda\psi(w_{t+1})] \leq \mathbb{E}[L(w_t) + \lambda\psi(w_t)] - \frac{\eta}{2} \mathbb{E}[\|\nabla L(w_t) + \lambda \nabla \psi(w_t)\|^2] + \frac{\eta^2 \beta}{2b} (\sigma^2 + \lambda^2 \sigma_\psi^2). \quad (16)$$

Proof. From the β -smoothness of L_{total} , we have:

$$\begin{aligned} & L(w_{t+1}) + \lambda\psi(w_{t+1}) \\ & \leq L(w_t) + \lambda\psi(w_t) + \mathbb{E}[\langle \nabla L(w_t) + \lambda \nabla \psi(w_t), w_{t+1} - w_t \rangle] + \frac{\beta}{2} \|w_{t+1} - w_t\|^2 \end{aligned}$$

Substituting the SGD update $w_{t+1} = w_t - \eta(\nabla L(w_t) + \lambda \nabla \psi(w_t))$, we obtain:

$$\begin{aligned} & L(w_{t+1}) + \lambda\psi(w_{t+1}) \\ & \leq L(w_t) + \lambda\psi(w_t) - \eta \langle \nabla L(w_t) + \lambda \nabla \psi(w_t), \nabla L(w_t) + \lambda \nabla \psi(w_t) \rangle \\ & \quad + \frac{\eta^2 \beta}{2} \|L(w_t) + \lambda\psi(w_t)\|^2 \end{aligned}$$

Taking the expectation, and noting that $\mathbb{E}[\nabla L_t(w_t)] = \nabla L(w_t)$ and then $\mathbb{E}[\nabla L_t(w_t) + \lambda \nabla \psi(w_t)] = \nabla L(w_t) + \lambda \nabla \psi(w_t)$, we get:

$$\begin{aligned} & \mathbb{E}[L(w_{t+1}) + \lambda \psi(w_{t+1})] \\ & \leq \mathbb{E}[L(w_t) + \lambda \psi(w_t)] - \eta \mathbb{E}[\langle \nabla L(w_t) + \lambda \nabla \psi(w_t), \nabla L(w_t) + \lambda \nabla \psi(w_t) \rangle] \\ & \quad + \frac{\eta^2 \beta}{2} \mathbb{E}[\|\nabla L_t(w_t) + \lambda \nabla \psi(w_t)\|^2] \\ & = \mathbb{E}[L(w_t) + \lambda \psi(w_t)] - \eta \mathbb{E}[\|\nabla L(w_t) + \lambda \nabla \psi(w_t)\|^2] + \frac{\eta^2 \beta}{2} \mathbb{E}[\|\nabla L_t(w_t) + \lambda \nabla \psi(w_t)\|^2] \end{aligned}$$

The stochastic gradient variance is bounded as:

$$\begin{aligned} & \mathbb{E}[L(w_{t+1}) + \lambda \psi(w_{t+1})] \\ & \leq \mathbb{E}[L(w_t) + \lambda \psi(w_t)] - \eta \mathbb{E}[\langle (\nabla L(w_t) + \lambda \nabla \psi(w_t)), (\nabla L_t(w_t) + \lambda \nabla \psi(w_t)) \rangle] \\ & \quad + \frac{\eta^2 \beta}{2} \mathbb{E}[\|(\nabla L_t(w_t) + \lambda \nabla \psi(w_t))\|^2] \\ & = \mathbb{E}[(L(w_t) + \lambda \psi(w_t))] - \eta \mathbb{E}[\|(\nabla L(w_t) + \lambda \nabla \psi(w_t))\|^2] + \frac{\eta^2 \beta}{2} \mathbb{E}[\|(\nabla L_t(w_t) + \lambda \nabla \psi(w_t))\|^2]. \end{aligned}$$

Expanding the variance term, we obtain

$$\begin{aligned} & \mathbb{E}[\|\nabla L_t(w_t) + \lambda \nabla \psi(w_t)\|^2] \tag{17} \\ & = \mathbb{E}[\|(\nabla L_t(w_t) + \lambda \nabla \psi(w_t)) - (\nabla L(w_t) + \lambda \nabla \psi(w_t)) + (\nabla L(w_t) + \lambda \nabla \psi(w_t))\|^2] \\ & = \mathbb{E}[\|\nabla L_t(w_t) - \nabla L(w_t)\|^2] + 2 \mathbb{E}[\langle \nabla L_t(w_t) - \nabla L(w_t), \nabla L(w_t) + \lambda \nabla \psi(w_t) \rangle] \\ & \quad + \mathbb{E}[\|\nabla L(w_t) + \lambda \nabla \psi(w_t)\|^2]. \tag{18} \end{aligned}$$

By the unbiasedness assumption (18) simplifies to

$$\mathbb{E}[\|\nabla L_t(w_t) + \lambda \nabla \psi(w_t)\|^2] = \mathbb{E}[\|\nabla L_t(w_t) - \nabla L(w_t)\|^2] + \mathbb{E}[\|\nabla L(w_t) + \lambda \nabla \psi(w_t)\|^2]. \tag{19}$$

By the gradient-variance bound assumption, we have

$$\mathbb{E}[\|(\nabla L_t(w_t) + \lambda \nabla \psi(w_t)) - (\nabla L(w_t) + \lambda \nabla \psi(w_t))\|^2] = \mathbb{E}[\|\nabla L_t(w_t) - \nabla L(w_t)\|^2] \leq \frac{\sigma^2 + \lambda^2 \sigma_\psi^2}{b}. \tag{20}$$

Combining (19) and (20), we obtain

$$\mathbb{E}[\|\nabla L_t(w_t) + \lambda \nabla \psi(w_t)\|^2] \leq \mathbb{E}[\|\nabla L(w_t) + \lambda \nabla \psi(w_t)\|^2] + \frac{\sigma^2 + \lambda^2 \sigma_\psi^2}{b}. \tag{21}$$

Substituting the variance bound (19)–(20) into the descent inequality yields:

$$\begin{aligned} & \mathbb{E}[L(w_{t+1}) + \lambda \psi(w_{t+1})] \\ & \leq \mathbb{E}[L(w_t) + \lambda \psi(w_t)] - \eta \mathbb{E}[\|\nabla L(w_t) + \lambda \nabla \psi(w_t)\|^2] \\ & \quad + \frac{\eta^2 \beta}{2} \left(\mathbb{E}[\|\nabla L(w_t) + \lambda \nabla \psi(w_t)\|^2] + \frac{\sigma^2 + \lambda^2 \sigma_\psi^2}{b} \right) \\ & = \mathbb{E}[L(w_t) + \lambda \psi(w_t)] - \eta \mathbb{E}[\|\nabla L(w_t) + \lambda \nabla \psi(w_t)\|^2] \\ & \quad + \frac{\eta^2 \beta}{2} \mathbb{E}[\|\nabla L(w_t) + \lambda \nabla \psi(w_t)\|^2] + \frac{\eta^2 \beta (\sigma^2 + \lambda^2 \sigma_\psi^2)}{2b} \\ & = \mathbb{E}[L(w_t) + \lambda \psi(w_t)] + \left(-\eta + \frac{\eta^2 \beta}{2} \right) \mathbb{E}[\|\nabla L(w_t) + \lambda \nabla \psi(w_t)\|^2] + \frac{\eta^2 \beta (\sigma^2 + \lambda^2 \sigma_\psi^2)}{2b} \\ & = \mathbb{E}[L(w_t) + \lambda \psi(w_t)] - \left(\eta - \frac{\eta^2 \beta}{2} \right) \mathbb{E}[\|\nabla L(w_t) + \lambda \nabla \psi(w_t)\|^2] + \frac{\eta^2 \beta (\sigma^2 + \lambda^2 \sigma_\psi^2)}{2b} \end{aligned}$$

Finally, given $\eta \leq \frac{1}{\beta}$, we have $\eta - \frac{\eta^2 \beta}{2} = \eta \left(1 - \frac{\eta \beta}{2} \right) \geq \frac{\eta}{2}$ and, since $\eta \beta \leq 1$ implies $1 - \frac{\eta \beta}{2} \geq \frac{1}{2}$.

Therefore,

$$\mathbb{E}[L(w_{t+1}) + \lambda \psi(w_{t+1})] \leq \mathbb{E}[L(w_t) + \lambda \psi(w_t)] - \frac{\eta}{2} \mathbb{E}[\|\nabla L(w_t) + \lambda \nabla \psi(w_t)\|^2] + \frac{\eta^2 \beta}{2b} (\sigma^2 + \lambda^2 \sigma_\psi^2)$$

□

Theorem 5. *Under the same smoothness and bounded-variance conditions stated in Lemma 4, and for a fixed step size $0 < \eta \leq 1/\beta$, the SGD update satisfies:*

$$\frac{1}{T} \sum_{t=0}^{T-1} \mathbb{E}[\|\nabla L(w_t) + \lambda \nabla \psi(w_t)\|^2] \leq \frac{2}{T\eta} ((L(w_0) + \lambda \psi(w_0))) - \frac{2}{T\eta} (\mathbb{E}[L(w_T) + \lambda \psi(w_T)]) + \frac{\eta \beta \sigma^2}{2b} + \frac{\lambda^2 \eta \beta \sigma_\psi^2}{2b}$$

Proof. Based on the descent lemma for classic SGD, we have:

$$\mathbb{E}[L(w_{t+1}) + \lambda \psi(w_{t+1})] \leq \mathbb{E}[L(w_t) + \lambda \psi(w_t)] - \frac{\eta}{2} \mathbb{E}[\|\nabla L(w_t) + \lambda \nabla \psi(w_t)\|^2] + \frac{\eta^2 \beta (\sigma^2 + \lambda^2 \sigma_\psi^2)}{2b} \quad (22)$$

Averaging (22) across T iterations, we obtain:

$$\begin{aligned} & \frac{1}{T} \sum_{t=0}^{T-1} \mathbb{E}[L(w_{t+1}) + \lambda \psi(w_{t+1})] \\ & \leq \frac{1}{T} \sum_{t=0}^{T-1} (\mathbb{E}[L(w_t) + \lambda \psi(w_t)]) - \frac{\eta}{2T} \sum_{t=0}^{T-1} \mathbb{E}[\|\nabla L(w_t) + \lambda \nabla \psi(w_t)\|^2] + \frac{1}{T} \sum_{t=0}^{T-1} \left(\frac{\eta^2 \beta (\sigma^2 + \lambda^2 \sigma_\psi^2)}{2b} \right) \end{aligned}$$

Rearranging the terms and substituting $\frac{1}{T} \sum_{t=0}^{T-1} (\mathbb{E}[L(w_t) + \lambda \psi(w_t)] - \mathbb{E}[L(w_{t+1}) + \lambda \psi(w_{t+1})]) = \frac{1}{T} (L(w_0) + \lambda \psi(w_0) - \mathbb{E}[L(w_T) + \lambda \psi(w_T)])$, we get:

$$\begin{aligned} & \frac{\eta}{2T} \sum_{t=0}^{T-1} \mathbb{E}[\|\nabla L(w_t) + \lambda \nabla \psi(w_t)\|^2] \\ & \leq \frac{1}{T} \sum_{t=0}^{T-1} (\mathbb{E}[L(w_t) + \lambda \psi(w_t)] - \mathbb{E}[L(w_{t+1}) + \lambda \psi(w_{t+1})]) + \frac{\eta^2 \beta (\sigma^2 + \lambda^2 \sigma_\psi^2)}{2b} \\ & = \frac{1}{T} ((L(w_0) + \lambda \psi(w_0)) - \mathbb{E}[L(w_T) + \lambda \psi(w_T)]) + \frac{\eta^2 \beta (\sigma^2 + \lambda^2 \sigma_\psi^2)}{2b} \end{aligned}$$

Dividing both sides by $\frac{\eta}{2}$, we obtain:

$$\begin{aligned} & \frac{1}{T} \sum_{t=0}^{T-1} \mathbb{E}[\|\nabla L(w_t) + \lambda \nabla \psi(w_t)\|^2] \\ & \leq \frac{2}{T\eta} ((L(w_0) + \lambda \psi(w_0)) - \mathbb{E}[L(w_T) + \lambda \psi(w_T)]) + \frac{\eta \beta (\sigma^2 + \lambda^2 \sigma_\psi^2)}{2b} \\ & \leq \frac{2}{T\eta} ((L(w_0) + \lambda \psi(w_0)) - \mathbb{E}[L(w_T) + \lambda \psi(w_T)]) + \frac{\eta \beta \sigma^2}{2b} + \frac{\lambda^2 \eta \beta \sigma_\psi^2}{2b} \end{aligned}$$

□

Corollary 6. *Under the same smoothness and bounded-variance assumptions stated in Lemma 4, and assuming further that L_{total} is bounded below by $L_{\text{total}}^{\text{inf}} > -\infty$, let the step size be constant $\eta = \frac{c}{\sqrt{T}}$ with $0 < c \leq \frac{1}{\beta}$. Then the SGD iterates satisfy:*

$$\frac{1}{T} \sum_{t=0}^{T-1} \mathbb{E}[\|\nabla L(w_t) + \lambda \nabla \psi(w_t)\|^2] \leq \frac{2((L(w_0) + \lambda \psi(w_0)) - L_{\text{total}}^{\text{inf}})}{c} T^{-1/2} + \frac{\beta c}{2b} (\sigma^2 + \lambda^2 \sigma_\psi^2) T^{-1/2}.$$

Proof. Starting from Theorem 5,

$$\frac{1}{T} \sum_{t=0}^{T-1} \mathbb{E}[\|\nabla L(w_t) + \lambda \nabla \psi(w_t)\|^2] \leq \frac{2}{T\eta} ((L(w_0) + \lambda \psi(w_0)) - \mathbb{E}[L(w_T) + \lambda \psi(w_T)]) + \frac{\beta \eta}{2b} (\sigma^2 + \lambda^2 \sigma_\psi^2). \quad (23)$$

Because $L(w_T) + \lambda\psi(w_T) \geq L_{\text{total}}^{\text{inf}}$, define $\Delta_0 = (L(w_0) + \lambda\psi(w_0)) - L_{\text{total}}^{\text{inf}}$. Substituting $\eta \leq \frac{c}{\sqrt{T}}$ yields

$$\begin{aligned} \frac{1}{T} \sum_{t=0}^{T-1} \mathbb{E} [\|\nabla L(w_t) + \lambda\nabla\psi(w_t)\|^2] &\leq \frac{2\Delta_0}{(c/\sqrt{T})T} + \frac{\beta c}{2b} (\sigma^2 + \lambda^2\sigma_\psi^2) T^{-1/2} \\ &= \frac{2\Delta_0}{c} T^{-1/2} + \frac{\beta c}{2b} (\sigma^2 + \lambda^2\sigma_\psi^2) T^{-1/2}. \end{aligned} \quad (24)$$

The overall convergence rate is $\mathcal{O}(\frac{1}{\sqrt{T}})$. □

Corollary 7 (Diminishing step size). *Under the same smoothness and bounded-variance assumptions stated in Lemma 4, and assuming further that the total objective $L(w) + \lambda\psi(w)$ is bounded below by $L_{\text{total}}^{\text{inf}} > -\infty$, consider SGD with a diminishing step-size sequence $(\eta_t)_{t \geq 0}$ satisfying:*

$$0 < \eta_t \leq \frac{1}{\beta}, \quad \sum_{t=0}^{\infty} \eta_t = \infty, \quad \sum_{t=0}^{\infty} \eta_t^2 < \infty.$$

Then the (step-size)-weighted average of squared gradients vanishes when $\nabla L_{\text{total}}(w_t) = \nabla L(w_t) + \lambda\nabla\psi(w_t)$:

$$\lim_{T \rightarrow \infty} \frac{1}{\sum_{t=0}^{T-1} \eta_t} \sum_{t=0}^{T-1} \eta_t \mathbb{E} [\|\nabla L_{\text{total}}(w_t)\|^2] = 0.$$

In particular,

$$\liminf_{T \rightarrow \infty} \min_{0 \leq t \leq T-1} \mathbb{E} [\|\nabla L_{\text{total}}(w_t)\|^2] = 0$$

Therefore, there exists a subsequence along which the expected squared gradient converges to 0.

Proof. From the β -smoothness of L_{total} and the SGD update $w_{t+1} = w_t - \eta_t(\nabla L_t(w_t) + \lambda\nabla\psi(w_t))$, the same argument as in the lemma yields, for any t with $\eta_t \leq 1/\beta$,

$$\mathbb{E}[L(w_{t+1})] \leq \mathbb{E}[L(w_t)] - \frac{\eta_t}{2} \mathbb{E} [\|\nabla L(w_t) + \lambda\nabla\psi(w_t)\|^2] + \frac{\beta \eta_t^2}{2b} (\sigma^2 + \lambda^2\sigma_\psi^2)$$

Summing from $t = 0$ to $T - 1$ and telescoping gives

$$\begin{aligned} \frac{1}{2} \sum_{t=0}^{T-1} \eta_t \mathbb{E} [\|\nabla L(w_t) + \lambda\nabla\psi(w_t)\|^2] &\leq \mathbb{E}[L(w_0)] - \mathbb{E}[L(w_T)] + \frac{\beta}{2b} (\sigma^2 + \lambda^2\sigma_\psi^2) \sum_{t=0}^{T-1} \eta_t^2 \\ &\leq (L(w_0) - L^{\text{inf}}) + \frac{\beta}{2b} (\sigma^2 + \lambda^2\sigma_\psi^2) \sum_{t=0}^{T-1} \eta_t^2. \end{aligned}$$

Divide both sides by $S_T := \sum_{t=0}^{T-1} \eta_t$ to obtain

$$\frac{1}{2S_T} \sum_{t=0}^{T-1} \eta_t \mathbb{E} [\|\nabla L(w_t) + \lambda\nabla\psi(w_t)\|^2] \leq \frac{(L(w_0) + \lambda\psi(w_0)) - (L + \lambda\psi)^{\text{inf}}}{S_T} + \frac{\beta}{2b} (\sigma^2 + \lambda^2\sigma_\psi^2) \frac{\sum_{t=0}^{T-1} \eta_t^2}{S_T}$$

By the step-size conditions, $S_T \rightarrow \infty$ and $\sum_{t=0}^{T-1} \eta_t^2 / S_T \rightarrow 0$ as $T \rightarrow \infty$. Hence the right-hand side tends to 0, which proves

$$\lim_{T \rightarrow \infty} \frac{1}{\sum_{t=0}^{T-1} \eta_t} \sum_{t=0}^{T-1} \eta_t \mathbb{E} [\|\nabla L(w_t) + \lambda\nabla\psi(w_t)\|^2] = 0.$$

Finally, since $\min_{0 \leq t \leq T-1} a_t \leq \frac{\sum_{t=0}^{T-1} \eta_t a_t}{\sum_{t=0}^{T-1} \eta_t}$ for any nonnegative sequence (a_t) , we get

$$\begin{aligned} \min_{0 \leq t \leq T-1} \mathbb{E} [\|\nabla L(w_t) + \lambda\nabla\psi(w_t)\|^2] &\leq \frac{\sum_{t=0}^{T-1} \eta_t \mathbb{E} [\|\nabla L(w_t) + \lambda\nabla\psi(w_t)\|^2]}{\sum_{t=0}^{T-1} \eta_t} \\ &\xrightarrow{T \rightarrow \infty} 0, \end{aligned}$$

which implies that even with the additional regularizer $\psi(w)$, the expected squared gradient is guaranteed to converge to 0 as $T \rightarrow \infty$. □

B Experimental Setups

B.1 Implementation Details

All experiments were conducted on four NVIDIA A40 GPUs (40GB each), with each model trained on a single GPU while multiple runs were executed in parallel across the four devices. The full training configurations, including model architectures, datasets, number of epochs, batch sizes, and regularization coefficients, are summarized in Tables B.1 and B.1.

Task	Model	Dataset	# Epochs	Batch Size	λ
Classification	ResNet-18 He et al. [2016]	CIFAR-10 Krizhevsky [2009]	200	128	1e-5
	ResNet-50 He et al. [2016]	SVHN Netzer et al. [2011]	200	128	1e-5
	WideRes28-10 Zagoruyko and Komodakis [2016]	CIFAR-100 Krizhevsky [2009]	200	128	1e-5
	ViT-B/32 Dosovitskiy et al. [2021]	CIFAR-100 Krizhevsky [2009]	200	128	1e-2
	ViT-B/32 Dosovitskiy et al. [2021]	Tiny-ImageNet CS231N [2015]	200	128	1e-2
Segmentation	Res50-Unet Ronneberger et al. [2015]	LGG MRI Buda et al. [2019]	200	64	1e-5

Table 7: Summary of datasets, network architectures, and training settings used in the experiments.

For classification tasks, we trained ResNet-18, ResNet-50, WideResNet-28-10, and ViT-B/32 for 200 epochs using a batch size of 128. Segmentation experiments on the LGG MRI dataset were performed using the ResNet50–UNet architecture for 200 epochs with a batch size of 64. The regularization strength λ for VAR was selected according to the dataset–architecture pair, as shown in Table B.1.

Task	Methods	Model	LR Initial	LR Scheduler	LR Decay Rate	ρ	Momentum	
Classification	SGD	Res-18/50 He et al. [2016], WideRes-28 Zagoruyko and Komodakis [2016]	0.1	Dynamic tuning	0.7	-	0.9	
	SFW Lu et al. [2022]	Res-18/50 He et al. [2016], WideRes-28 Zagoruyko and Komodakis [2016]	1.0	Dynamic tuning	0.7	-	0.9	
	CrAM Chen et al. [2023]	Res-18/50 He et al. [2016], WideRes-28 Zagoruyko and Komodakis [2016]	0.1	Dynamic tuning	0.7	0.05	0.9	
	SAM Foret et al. [2021]	Res-18/50 He et al. [2016], WideRes-28 Zagoruyko and Komodakis [2016]	0.1	Dynamic tuning	0.7	0.5	0.9	
	SGD	ViT-B/32 Dosovitskiy et al. [2021]	0.001	Dynamic tuning	0.7	-	0.9	
	SFW Lu et al. [2022]	ViT-B/32 Dosovitskiy et al. [2021]	-	-	-	-	-	
	CrAM Chen et al. [2023]	ViT-B/32 Dosovitskiy et al. [2021]	0.001	Dynamic tuning	0.7	0.05	0.9	
	SAM Foret et al. [2021]	ViT-B/32 Dosovitskiy et al. [2021]	0.001	Dynamic tuning	0.7	0.25	0.9	
	Segmentation	SGD	Res50-Unet Ronneberger et al. [2015]	0.01	Step Decay	0.5	-	0.9
		SFW Lu et al. [2022]	Res50-Unet Ronneberger et al. [2015]	0.01	Step Decay	0.5	-	0.9
CrAM Chen et al. [2023]		Res50-Unet Ronneberger et al. [2015]	0.01	Step Decay	0.5	0.05	0.9	
SAM Foret et al. [2021]		Res50-Unet Ronneberger et al. [2015]	0.01	Step Decay	0.5	0.25	0.9	

Table 8: Training configurations for all experiments, including the optimizer type, network architecture, initial learning rate, learning rate scheduling strategy, decay rate, momentum, and optimizer-specific hyperparameters used in both classification and segmentation tasks. Here, “-” denotes settings that are not applicable for a given method.

Learning Rate Scheduling. The learning rate strategies differ between classification and segmentation tasks:

- **Dynamic Tuning (Classification).** The learning rate is reduced by a factor of 10 at one-third and two-thirds of the total training epochs. After epoch 20, the learning rate is additionally adjusted every five epochs using a moving-loss comparison: if the recent 5-epoch loss average exceeds the recent 10-epoch average, the learning rate is multiplied by 0.7; otherwise it is slightly increased by multiplying by 1.06.
- **Step Decay (Segmentation).** A standard step-decay rule is used, multiplying the learning rate by 0.5 every 50 epochs.

All SFW experiments use the official default configuration provided in the public repository, including an initial learning rate of 1.0, the dynamic_change learning rate scheduling mode, momentum of 0.9, zero weight decay, a k -sparse polytope constraint with $K = 10$ and $K_{\text{frac}} = 0.05$, diameter parameter $\tau = 15$, constraint rescaling mode set to initialization, and the SFW_Init option disabled. For constrained updates, SFW performs projection onto the k -sparse polytope at every optimization step. CrAM, and SAM also follow the default settings specified in their official repositories. However, for ViT-B/32 and the ResNet50–UNet segmentation model, the default perturbation radius $\rho = 0.5$ in SAM led to unstable training. We therefore selected a smaller ρ by gradually reducing the value and choosing the one that yielded the highest F1-score.

B.2 Benchmark Datasets

This work evaluates the proposed Variance Amplifying Regularizer (VAR) across two major task categories: image classification and medical image segmentation. All experiments are conducted in a single-model setting without any fine-tuning after pruning.

Image Classification. We assess pruning robustness on four widely used classification benchmarks that offer diverse image statistics and class granularities:

- **CIFAR-10** Krizhevsky [2009]: A natural image dataset of 32×32 RGB images containing 10 general object categories.
- **CIFAR-100** Krizhevsky [2009]: An extension of CIFAR-10 with the same 32×32 resolution but expanded to 100 fine-grained categories.
- **SVHN** Netzer et al. [2011]: A real-world digit classification dataset derived from street-view house numbers, consisting of 32×32 RGB images across 10 digit classes.
- **Tiny-ImageNet** CS231N [2015]: A subset of ImageNet composed of 64×64 RGB images spanning 200 object categories, offering a more challenging mid-scale benchmark.

Image Segmentation. We further evaluate pruning robustness on a medical image segmentation benchmark that requires pixel-level prediction under a structurally sensitive setting:

- **LGG Brain MRI Dataset** Buda et al. [2019]: A collection of brain MRI scans from lower-grade glioma patients, each paired with expert-annotated tumor masks for pixel-wise segmentation.

B.3 Evaluation Metrics

This section summarizes the evaluation metrics used across the classification and segmentation experiments. All metrics follow the official definitions provided by each benchmark, ensuring consistency with prior work.

Image Classification. For all classification benchmarks, model performance is measured using the standard *test accuracy* (*Acc*). Accuracy reflects the proportion of correctly predicted samples over the entire test set and is widely adopted as the primary metric for CIFAR-10, CIFAR-100, SVHN, and Tiny-ImageNet.

Image Segmentation. For segmentation on the LGG Brain MRI dataset, we use three complementary metrics to assess mask quality:

- **F1-score (F1):** Measures the harmonic mean of precision and recall, capturing overall overlap between prediction and ground truth.
- **Tversky Index:** A generalization of the Dice score that asymmetrically penalizes false positives and false negatives, enabling robust evaluation under class imbalance.
- **Hausdorff Distance (H-Dist.):** Quantifies the largest boundary deviation between the predicted mask and ground truth, with lower values indicating more accurate boundary localization.

These metrics jointly evaluate segmentation completeness, precision, and boundary alignment.

B.4 One-shot Pruning Method.

All pruning is performed in a *one-shot* manner, applied once after full training without any retraining or fine-tuning. In convolutional networks, convolutional weights are globally pruned using an L_1 magnitude threshold. For vision transformers, pruning is applied to the self-attention and feed-forward modules using two configurations: (P1) equal pruning across Query, Key, Value, Projection, and FFN layers, and (P2) slightly adjusts the ratio by pruning FFN layers 3% more while pruning the remaining (QKV and Projection) layers proportionally less, maintaining the same overall pruning rate.

In the appendix, we further extend the pruning analysis by evaluating ViT models under pruning configurations that selectively prune only the Q, QK, or QKV components in Section C.3. These additional experiments provide a more

fine-grained understanding of how pruning different subsets of the attention mechanism affects model robustness under various sparsity levels.

C Experimental results

This section presents additional experimental results that complement the findings reported in the main paper.

C.1 Additional Results with Aggressive Pruning

Table C.1 reports additional classification results conducted at pruning rates higher than those presented in the main paper. These experiments evaluate pruning robustness at extreme sparsity levels (96–98%) on CIFAR-10 and SVHN using ResNet-18 and ResNet-50.

Pruning Rate	Method VAR (Ours)	CIFAR-10		SVHN	
		ResNet-18		ResNet-50	
		w/o	w	w/o	w
Dense	SGD	92.75	92.76	94.44	94.56
	SFW Lu et al. [2022]	92.54	92.34	95.79	95.80
	CrAM Chen et al. [2023]	94.19	93.86	95.97	95.79
	SAM Foret et al. [2021]	95.19	94.01	96.96	95.98
96%	SGD	19.69	21.53	9.15	6.37
	SFW Lu et al. [2022]	84.15	89.93	18.20	95.49
	CrAM Chen et al. [2023]	66.66	81.72	27.78	31.26
	SAM Foret et al. [2021]	48.36	92.08	9.74	95.99
97%	SGD	19.22	20.30	9.15	6.37
	SFW Lu et al. [2022]	59.12	66.52	6.69	9.69
	CrAM Chen et al. [2023]	35.0	69.08	11.34	12.86
	SAM Foret et al. [2021]	36.87	87.33	9.69	95.90
98%	SGD	15.32	16.31	9.15	6.37
	SFW Lu et al. [2022]	12.61	15.02	6.69	9.69
	CrAM Chen et al. [2023]	17.27	41.77	6.87	8.47
	SAM Foret et al. [2021]	21.54	54.56	9.75	95.59

Table 9: Accuracy comparison (%) across high pruning rates and datasets (CIFAR-10, SVHN) using ResNet18/50, with and without VAR, denoted as “w/o” and “w.”

Across all settings, the proposed VAR consistently improves accuracy under very high pruning, even when baseline performance collapses. The gains are most prominent when coupled with SAM, where VAR preserves most of the dense-model performance despite removing up to 98% of the weights.

C.2 Additional Segmentation Results

To further examine the effect of the proposed Variance Amplifying Regularizer (VAR) under high pruning rates, we provide additional qualitative segmentation results in Figure 4 and Figure 5. Each figure compares the segmentation masks produced by several pruning-robust training methods, both with and without VAR, alongside the corresponding ground-truth tumor annotations.

Across all examples, models trained without VAR often show degraded predictions after 85% one-shot pruning. Typical failure patterns include incomplete tumor regions, loss of boundary continuity, and irregular or noisy shapes. In contrast, models trained with VAR consistently preserve more complete lesion structures and maintain clearer and more accurate tumor boundaries. Methods such as SFW and SAM particularly benefit from the addition of VAR, which stabilizes the model’s internal representations even under severe sparsity.

These qualitative findings are consistent with the quantitative results presented in the main paper. By promoting broader and more structured weight distributions during training, VAR reduces the distortion caused by aggressive pruning and leads to better segmentation masks, especially for tumors with complex shapes or low-contrast regions.

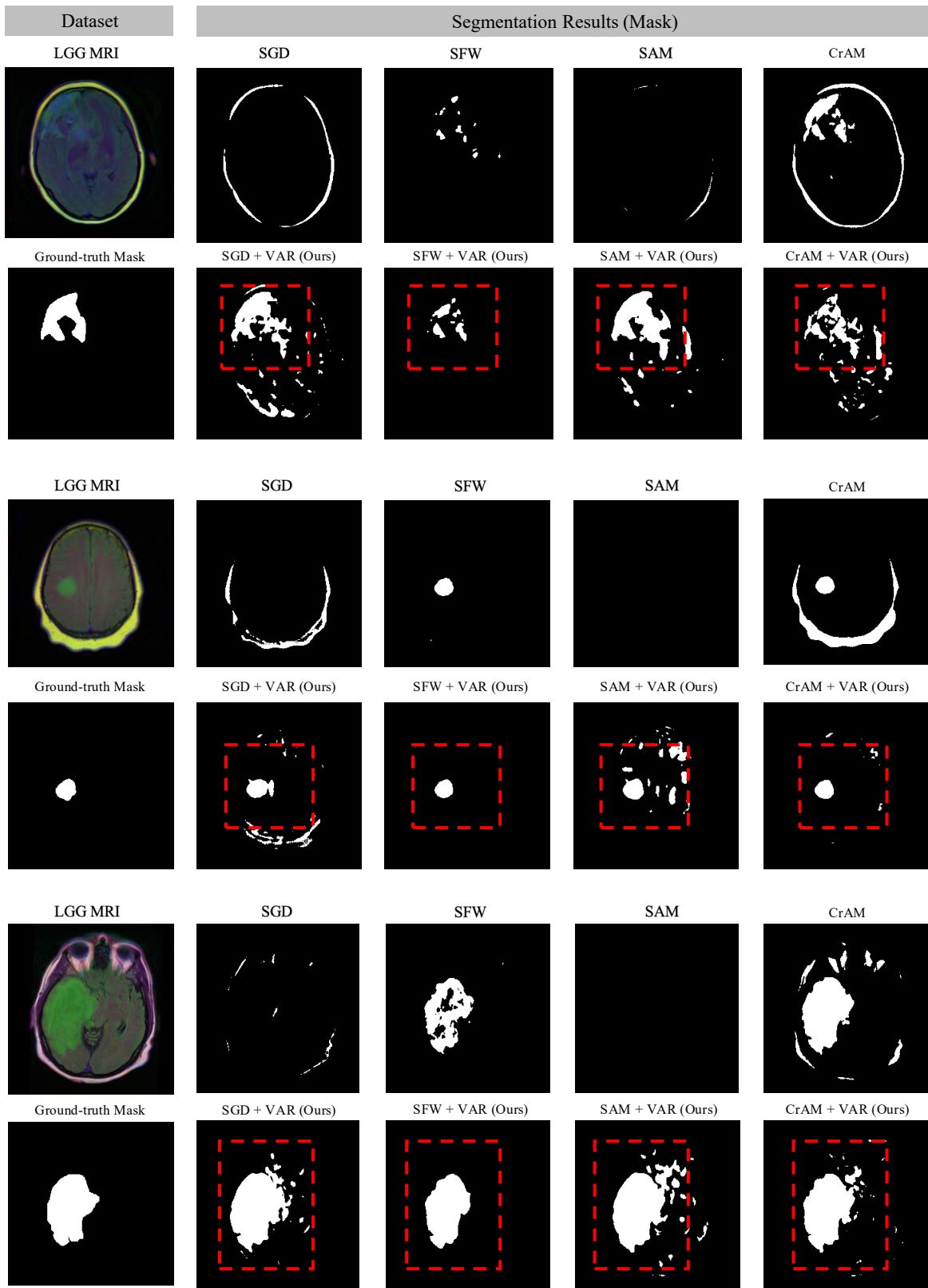


Figure 4: Qualitative segmentation results on the LGG MRI dataset using the ResNet-50–UNet architecture under 85% pruning. Each column displays the outputs of different pruning-robust training methods, shown both with and without our proposed Variance Amplifying Regularizer (VAR), along with the corresponding ground-truth mask.

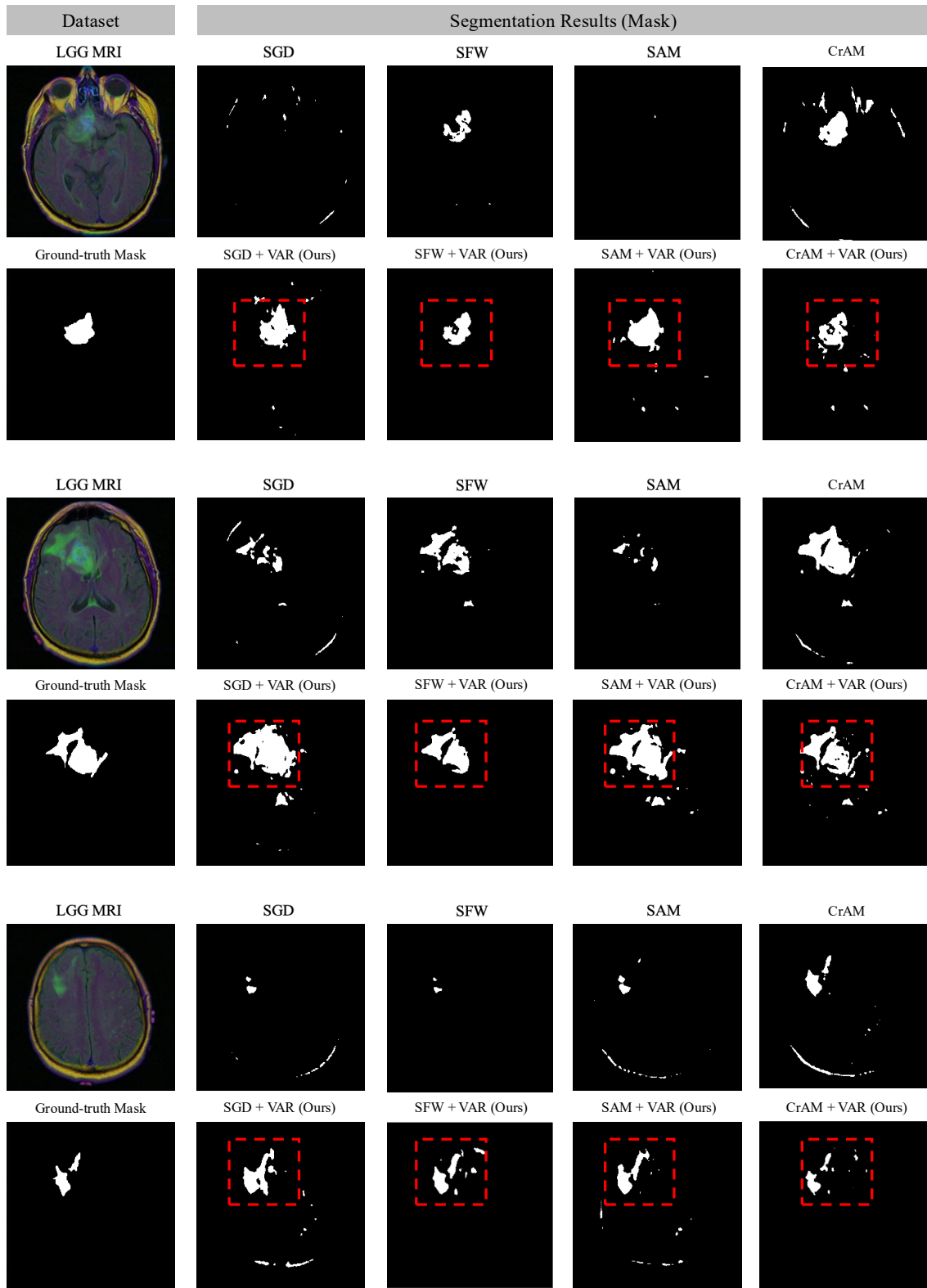


Figure 5: Qualitative segmentation results on the LGG MRI dataset using the ResNet-50–UNet architecture under 85% pruning. Each column displays the outputs of different pruning-robust training methods, shown both with and without our proposed Variance Amplifying Regularizer (VAR), along with the corresponding ground-truth mask.

C.3 Ablation Study

We examine the effect of the regularization coefficient λ on pruning robustness for both CNNs (ResNet-18 on CIFAR-10) and Vision Transformers (ViT-B/32 on CIFAR-100).

Method		SGD								SAM							
Pruning Rate	λ	NA	1e-6	5e-6	1e-5	5e-5	1e-4	5e-4	1e-3	NA	1e-6	5e-6	1e-5	5e-5	1e-4	5e-4	1e-3
	$Var(w)$	0.0019	0.0021	0.0030	0.0035	0.0060	0.0081	0.0165	0.0226	0.00005	0.00010	0.00018	0.00024	0.00050	0.00069	0.00151	0.00212
Dense		92.75	93.14	91.87	92.76	92.79	91.62	90.54	90.66	95.19	94.65	94.11	94.01	92.77	91.93	90.75	90.29
60%		91.66	92.93	91.61	92.0	92.61	91.59	90.44	90.54	95.19	94.65	94.11	94.01	92.77	91.93	90.75	90.29
70%		91.66	92.40	91.39	91.82	92.05	90.72	89.79	90.08	95.11	94.65	94.11	94.01	92.77	91.93	90.75	90.29
80%		85.93	90.36	89.77	91.14	90.29	85.86	84.75	82.16	94.72	94.63	94.11	94.01	92.77	91.93	90.75	90.29
90%		43.57	68.55	77.00	80.51	76.73	64.87	66.22	58.22	91.26	94.47	94.22	94.04	92.77	91.93	90.75	90.29
92%		31.60	57.53	65.47	70.18	68.05	53.47	52.11	47.39	87.20	94.15	94.04	93.91	92.72	91.93	90.77	90.29
94%		26.10	41.02	51.0	50.25	49.56	41.62	31.5	35.25	76.29	92.61	93.69	93.77	92.69	91.90	90.76	90.08
96%		19.69	24.53	36.79	21.53	20.60	21.72	12.75	20.18	48.36	84.54	91.91	92.08	92.50	91.61	89.75	87.72

Table 10: Performance comparison across different regularization coefficient (λ) values on CIFAR-10 with ResNet-18. The column labeled *NA* denotes the baseline without the variance regularizer.

Pruning Rate	λ	Q-Pruning						QK-Pruning						QKV-Pruning					
		N/A	1e-5	1e-4	1e-3	1e-2	1e-1	N/A	1e-5	1e-4	1e-3	1e-2	1e-1	N/A	1e-5	1e-4	1e-3	1e-2	1e-1
	$Var(w)$	0.0070	0.0070	0.0073	0.0101	0.0209	0.0574	0.0070	0.0070	0.0073	0.0101	0.0209	0.0574	0.0070	0.0070	0.0073	0.0101	0.0209	0.0574
Dense		89.84	90.00	90.15	89.62	88.75	85.23	89.84	90.00	90.15	89.62	88.75	85.23	89.84	90.00	90.15	89.62	88.75	85.23
60%		89.52	89.75	89.70	89.43	88.65	85.23	88.75	89.25	89.11	89.29	88.79	85.23	86.30	86.68	87.29	88.23	88.58	85.23
70%		88.88	89.15	89.19	89.04	88.58	85.16	87.09	87.23	87.47	88.29	88.11	85.15	78.33	78.76	80.45	84.83	85.66	83.81
80%		87.57	87.63	87.95	88.15	87.90	84.69	79.52	80.72	81.65	84.90	86.06	84.16	51.13	52.93	55.48	69.63	73.69	68.11
90%		80.29	81.27	81.51	83.84	85.13	82.75	51.54	52.61	54.57	65.31	73.41	75.01	9.55	12.18	11.14	15.00	14.63	5.07
92%		76.25	77.44	77.68	81.22	83.04	81.22	41.56	43.22	43.84	54.82	64.43	50.61	7.23	7.83	7.75	9.21	8.82	2.84
94%		68.97	70.52	70.66	76.48	78.88	78.54	31.67	33.52	33.45	41.31	50.65	33.18	5.07	6.02	5.27	6.29	3.32	1.78
96%		56.31	57.86	58.25	66.83	70.33	71.73	23.32	24.75	24.06	27.64	33.25	19.52	3.04	4.42	3.62	4.61	2.31	1.51

Table 11: Performance comparison of ImageNet-Pretrained Vision Transformer (ViT-B/32) models on CIFAR-100 under different pruning configurations and regularization strengths λ . Each column shows results for Q, QK, and QKV-pruning, where pruning is applied respectively to the Query, Query–Key, and Query–Key–Value within the self-attention mechanism.

CNNs (ResNet-18). Varying λ directly controls the parameter variance $Var(w)$ and leads to clear differences in pruning stability. Small to moderate values (10^{-6} , 10^{-5}) consistently improve accuracy across pruning rates, especially in the high-pruning regime, while excessively large values degrade dense accuracy.

ViTs (ViT-B/32). Transformers benefit from stronger regularization due to their larger parameterization and reliance on attention pathways. Increasing λ yields higher pruning robustness across all sparsity levels, and optimal performance is typically achieved with λ in the range of 10^{-3} , 10^{-2} . The appendix further evaluates ViT pruning restricted to specific attention components (Q, QK, and QKV pruning). Across all three configurations, larger λ values consistently enhance robustness, showing that variance amplification improves structural stability even when pruning targets only subsets of the self-attention mechanism.

Overall, λ serves as a controllable factor governing the strength of variance amplification. CNNs require smaller regularization, while ViTs benefit from stronger penalties, demonstrating that optimal λ scales naturally with model size and architecture.

D PyTorch Implementation

```
def variance_regularization(model, lambda_var=0.01):
    variance_loss = torch.tensor(0.0, device=next(model.parameters()).device)
    lambda_var = float(lambda_var)
    for param in model.parameters():
        if param.requires_grad and len(param.shape) > 1:
            abs_param = param.abs()
            mean_param = abs_param.mean()
            var_param = ((abs_param - mean_param) ** 2).mean()
            variance_loss += lambda_var / (var_param + 1e-8)
    return variance_loss
```

Figure 6: PyTorch implementation of the proposed Variance Amplifying Regularizer (VAR). For each layer, the regularizer computes the reciprocal of the variance of the absolute weight values, encouraging wider weight distributions that improve pruning robustness. The final regularization loss is the sum of these layer-wise terms.